Hindawi
International Journal of Aerospace Engineering
Volume 2022, Article ID 5216387, 18 pages
https://doi.org/10.1155/2022/5216387

Research Article

Design Improvement of a BWB Aerodynamic Performance at Cruise and Take-Off Speeds

Gang Yu [1,2] **and Yuling Duan** [3]

[1]*School of Mechanical Engineering, Hubei University of Arts and Science, Xiangyang, 441053 Hubei, China*
[2]*Hubei Longzhong Laboratory, 441000 Hubei, China*
[3]*AVIC Aerospace Life-Support Co. Ltd., Xiangyang, 441053 Hubei, China*

Correspondence should be addressed to Gang Yu; yugang@hbuas.edu.cn

Received 2 June 2022; Revised 5 November 2022; Accepted 7 November 2022; Published 23 November 2022

Academic Editor: Kenneth M. Sobel

As a high-performance aircraft, BWB (blended wing body) has attracted the attention of many countries around the world. A 300-seat BWB design is proposed by the Airplane Concept Design Institute of Northwestern Polytechnical University, which is also called SWB. The aerodynamic performance of it is evaluated by CFD (computational fluid dynamics). The CFD calculation method is based on RANS (Reynolds-averaged Navier–Stokes), and it is verified by wind tunnel test results at take-off speed. However, the aerodynamic design of the SWB needs to be improved to meet the market demand to increase its cruise Mach number from 0.8 to 0.85. To achieve this goal, firstly, based on the previous calculation and analysis results, the basic shape of SWB is improved by using "aft-body extending" technology and discrete adjoint optimization method. Then, the winglets are applied to the improved basic shape to improve its cruise speed aerodynamic performance, and the Krueger flaps are applied as its high-lift device to improve its take-off and landing aerodynamic performance. The CFD calculation and wind tunnel test results show that these improvements make SWB-2 have a good aerodynamic performance at the Mach number of 0.85. Therefore, these design improvements are appropriate and effective for improving the aerodynamic performance of BWB.

1. Introduction

For many years, embodied in the B-47 are most of the fundamental design features of the conventional subsonic jet transport: cylinder body, trapezoidal wing, empennage, and podded engines hung on pylons beneath and forward of the wing [1]. However, at the time of designing the B747, it has been believed that the typical configuration with a cylindrical body has reached its maximum performance, and further development for commercial transport could be a challenge [2]. Therefore, to obtain a significant increase in performance, a nonconventional blended wing body (BWB) aircraft is proposed by manufacturers and universities [3].

The BWB aircraft is a tailless design that integrates the wing and the fuselage [4]. It represents a potential revolution in subsonic transport efficiency for large airplanes [5]. By blending a lift-generating center-body housing payload with conventional outer wings [6], BWB obtains a compact aerodynamically efficient flying wing providing structural, aerodynamic, and payload synergy, offering high lift-to-drag ratio (L/D), low fuel cost, and low noise [7, 8]. An increase in $(L/D)_{\max}$ of about 20% over the conventional design has been estimated for the BWB. However, these benefits can only be realized as an improved aerodynamic performance through careful and detailed aerodynamic shape design [4].

As a high-performance aircraft, BWB is very suitable for "Green Aviation" [9]. With the emphasis on the environment and the pursuit of high-performance aircraft, BWB has attracted the attention of many countries around the world [10, 11]. In 1997, a 17 ft span model aircraft—BWB-17 designed by Boeing combined with NASA and Stanford University—demonstrated the feasibility of BWB [12, 13]. And then, in 2003, following the success of the BWB-17, through a three-year project and lots of joint researches, a 450-passenger capacity commercial transport BWB-450

(Figure 1(a)) was led to birth by Boeing and NASA [14]. The BWB-450 was designed with a multidisciplinary design tool, WingMOD. By using three boundary layer ingestion (BLI) engines, the fuel burn per seat of BWB-450 can be reduced by about 30% [15].

From 2002 to 2012, the European Union (EU) obtained a series of BWB configurations through the 5th, 6th, and 7th Framework Programs. The 5th EU Framework Program consists of the Multidisciplinary Optimization of a Blended Wing Body (MOB) and the Very Efficient Large Aircraft (VELA) projects. The MOB project created a computational design engine (CDE) for the multidisciplinary design and optimization of a BWB. The VELA project gave rise to VELA 1, VELA 2, and VELA 3. The design cruise Mach number of VELA 3 is 0.85 and range is 7200 nm. The 6th Framework Program is also named as NACRE (New Aircraft Concept Research). NACRE PFW1 and PFW2 (Figure 1(b)) are derived from VELA 3 by some design changes [7]. The 7th Framework Programs is called the Active Flight Control for Flexible Aircraft 2020 (ACFA2020). A 450-capacity BWB with 2 podded turbofan engines were designed from this project. Russia has also proposed its BWB configurations, such as "IWB-750" based on the VELA configuration [9]. The maximum lift-to-drag (L/D) ratio of IWB can reach 25 at its cruise Mach 0.85.

In 2002, the Silent Aircraft Initiative (SAI) was funded by the Cambridge-MIT Institute. The SAX-12, SAX-29, and finally SAX-40 in 2006 were led to birth by the SAI plan [16]. The SAI was further explored during the NASA sponsored N+2 research at MIT [17]. In 2007, based on SAX-40, Boeing proposed two configurations for N+2 (N2A and N2B), as shown in Figure 2. However, the N2A is with podded engines, and the N2B still remains the SAX-40 embedded engine [18]. In 2008, MIT proposed H3 configuration for N+3. Although the H3 final design achieves neither the N+3 noise nor fuel efficiency goals, it achieves all N+2 goals with a relatively conventional propulsion system [19].

In China, a 300-seat BWB was proposed by the team of Airplane Concept Design Institute of Northwestern Polytechnical University (NPU-ACDI) in 2011 [20, 21]. It is called the ship-shaped wing (SWB) for its body looks like a ship, as shown in Figure 3. Flight tests, wind tunnel tests, and computational fluid dynamics (CFD) are the main methods used to study the aircraft aerodynamic performance. Among these, numerical simulations are less expensive and more efficient and can obtain full flow-field information. The aerodynamic performance of SWB was evaluated by CFD [22]. The grid generation software used in this paper is ICEM, and the CFD calculation software is CFD++. In addition, wind tunnel tests were also used to verify the CFD calculation results of some typical states.

2. The Aerodynamic Performance of SWB

The wingspan of SWB is about 63.1 m, and the length of it is about 40.8 m. The planform of SWB and the airfoil shape of its spanwise control sections are shown in Figure 4. There are nine control airfoils in SWB spanwise direction. Airfoils 1-4 are located in the center body, and preloading reflex airfoils are used to improve trim requirements; airfoils 4-6 are located in the blending area and reflex airfoils are used to minimise loading at the junction; airfoils 6-9 are located in the outer wing, and supercritical airfoils are used for washout arrangement [1, 23]. The coordinates of x and z represent the chordwise and spanwise positions, c_r represents the root chord of BWB, and B represents the half-span length [24]. For the sake of simplicity, a linear interpolation of adjacent airfoils is applied to construct the 3D geometry of BWB configuration.

The governing equation of the CFD method used to evaluate the SWB aerodynamic performance is the 3D RANS equation as follows:

$$\frac{\partial}{\partial t}\iiint_V W dV + \oiint_\Omega (H_c gn - H_v gn) dS = 0, \quad (1)$$

where $W = \{\rho, \rho u, \rho v, \rho w, \rho E\}^T$ represents the flow-field conservation term, H_c represents the inviscid flux terms, H_v represents the viscous flux term, n is the external normal vector of the boundary Ω of the control volume element, V represents the volume, and S represents the surface area.

The finite volume method is used to solve the RANS equations. Its inviscid term is discretized by the second-order upwind Roe FDS scheme, and the viscid term is discretized by the second-order central difference scheme. The turbulence model used is k-omega SST model. The time-stepping method is an approximate factorization (AF) implicit time-marching method; the multigrid method is applied to accelerate the convergence process of calculation [25].

The grid of SWB used for CFD calculation is a multiblock O-H structure grid with about 4.2 million cells, as shown in Figure 5. The far field boundary is located 10 body lengths from the configuration. The boundary condition used on all solid surfaces is no-slip adiabatic wall condition.

2.1. The Aerodynamic Performance of SWB at Take-Off Speed. The CFD calculation results at take-off speed (0.2 Ma, low speed) are compared with the wind tunnel test results to verify the feasibility of CFD calculation method. The wind tunnel test was done in NPU NF-3 wind tunnel using a 1/25 smaller model. The test Reynolds number is 4.67×10^6. The model installed in the wind tunnel is shown in Figure 6. The aerodynamic force coefficient results of wind tunnel test and CFD analysis are shown in Figure 7. It can be seen from the results that the stalling characteristic of SWB is soft, and the CFD results are in good agreement with the wind tunnel test results except the pitching moment coefficient at high angles of attack. However, the development trend of the pitch moment coefficient of CFD and wind tunnel test is the same under high angle of attack. Therefore, although the pitching moment coefficient value is slightly different from that of wind tunnel test at high angle of attack, the CFD analysis method used in this paper is feasible.

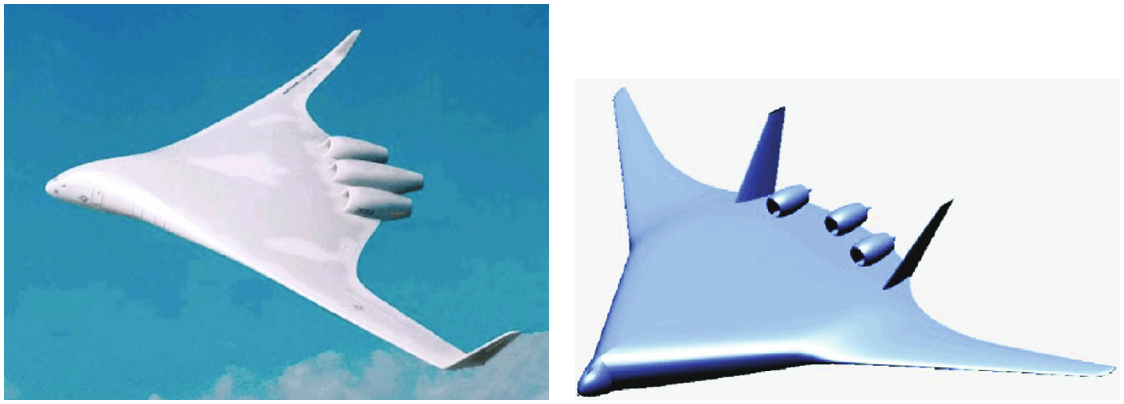

(a) BWB-450 (b) NACRE PFW-2

Figure 1: BWB-450 and NACRE PFW-2 configurations [7].

(a) N2A (b) N2B

Figure 2: N2A and N2B configurations [18].

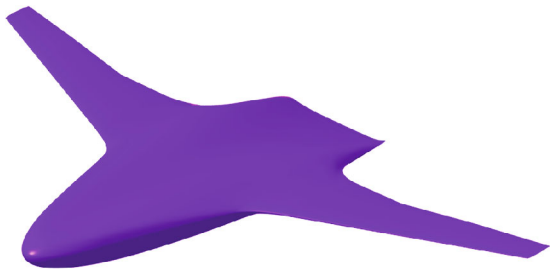

Figure 3: The SWB configuration.

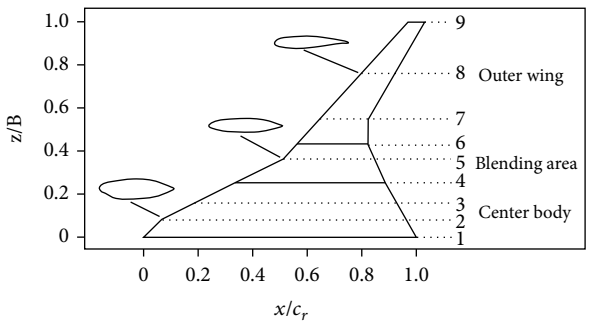

Figure 4: The planform and airfoils of SWB.

Figure 8 shows the SWB surface streamline results from the wind tunnel silk thread technology and CFD analysis results at angle of attack at $\alpha = 8^\circ$, 10°, and 14°.

It can be seen from the results that at $\alpha = 8^\circ$, the silk thread and CFD results indicate that the air flow over the body and wing is attached, but the spanwise flow caused by the large sweep back angle of the center body begins to affect the blending area; at $\alpha = 10^\circ$, with the strength of spanwise flow, a small flow separation region occurs at the leading edge of the blending area; meanwhile, the stability of the blending area boundary is getting worse, the silk swing scope to out wing is getting bigger, but the air flow over the wing is still attached. The CFD results are consistent with the silk thread; at $\alpha = 14^\circ$, except for the silk on the wingtip, most of the silk on the wing clearly swings to the leading edge. It indicates that the flow separation is growing larger, and the lift has reached to the top. The CFD results can also show a larger backflow area. It can be seen that the silk on the back of the center body is still attached, indicating that the positively cambered trailing edge is appropriate.

The surface pressure contour of SWB at different angle of attack is shown in Figure 9. It can be seen that with the angle of attack increase, the flow separation will enlarge the low-pressure area at the wing body blended area and make the pressure distribution at the tail of the outer wing uneven. Because RANS has limitations in simulating separated flow, there is a little difference between the pitch

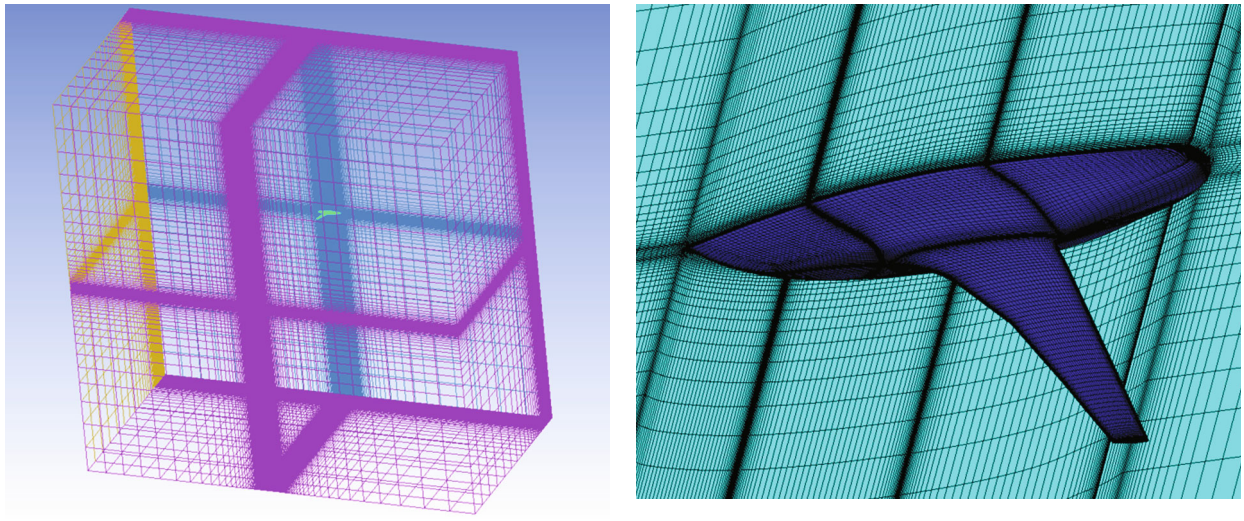

(a) Volume grid (b) Surface grid

Figure 5: The grid of SWB.

Figure 6: SWB wind tunnel model.

moment coefficient results of CFD and wind tunnel test results.

2.2. The Aerodynamic Performance of SWB at High Speed. Some typical aerodynamic characteristic curves of the SWB at high speed at 11 km are shown in Figure 10. It can be seen that the aerodynamic efficiency factor of SWB reaches to the maximum (as shown in Figure 10(e)) at Ma = 0.8, $\alpha = 2\circ$, and at this point, the $L/D\,(K)$ ratio of SWB is more than 28, $C_L = 0.2$, $C_M < 0$; the slope of the C_M curve is negative and has good linearity near this point. Therefore, SWB has good aerodynamic performance at this point, Ma = 0.8 can be the cruise Mach number of SWB, and $\alpha = 2\circ$ can be the cruise angle of attack of SWB. Moreover, the drag divergence Mach number of SWB is about 0.83 at $C_L = 0.2$.

The surface pressure contour of SWB at different Mach number at cruise lift coefficient $C_L = 0.2$ is shown in Figure 11. It could be seen that the SWB configuration is basically shock-free at the cruise Mach number. The shock wave strength at blended and wing area becomes larger with Mach number increases, and position of the shock wave changes back forward. However, the flow on the center body is always isentropic shock-free flow; this is because of two reasons: the large leading edge sweep back angle of the center body and the reduced relative thickness of the long center body.

In general, from the high-speed aerodynamic performance analysis, it represents that the SWB has good aerodynamic performance at Ma = 0.8. However, as the drag divergence Mach number of SWB is about 0.83, the aerodynamic performance of SWB is not good at Ma = 0.85. Most BWB designs have used Mach 0.85 as a cruise design point as this is consistent with current large transport aircraft operation [4]. Moreover, according to Liebeck [26], BWB at this Mach number has the maximum payload efficiency. Therefore, there was a requirement to design a BWB with a cruise Mach number of 0.85. The aerodynamic performance of SWB at Ma = 0.85 needed to be improved.

3. Improvement of SWB Aerodynamic Design

3.1. Basic Shape Improvement. To make SWB more competitive in the market, the cruise Mach number of SWB needs to be increased to 0.85. From Figure 10, it can be known that the drag divergence Mach number of SWB is below 0.85, and at 0.85 Ma, the SWB maximum L/D is about 17 at 1.5°. It is slightly lower for the BWB, which has good aerodynamic efficiency [27]. Therefore, the SWB aerodynamic design needs to be improved [28].

Theoretically, aerodynamic optimization design can solve this problem very well. However, if the correct optimization direction is unknown, it can take a lot of time to find the optimal result from a large number of optimization parameters and a big optimization space. To improve the optimization efficiency, some empirical improvements are firstly applied to the SWB basic shape. Then, the aerodynamic optimization is based on the improved basic shape.

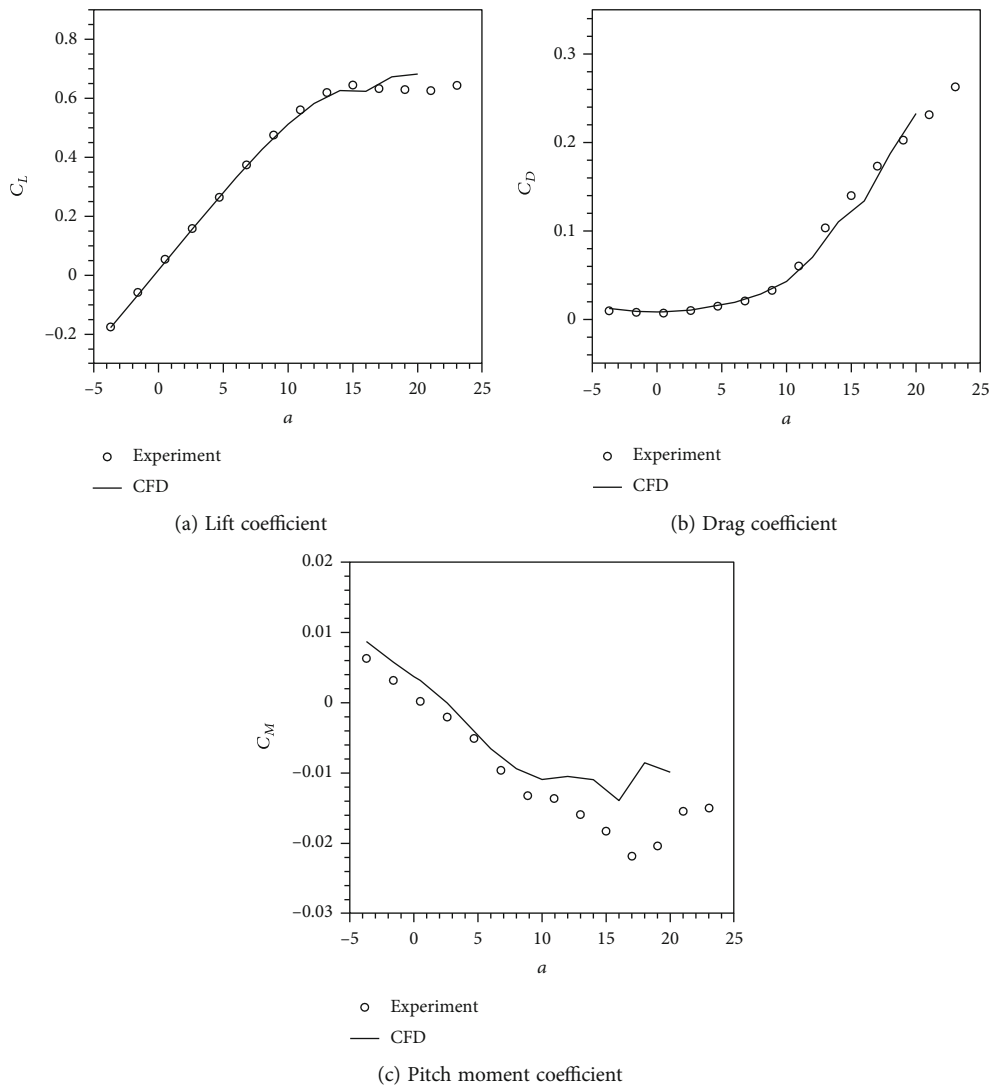

Figure 7: Typical aerodynamic characteristic curves of SWB at take-off speed.

As can be seen from Figure 11, due to the increase of Mach number, the shock wave on SWB upper surface moves from the leading edge to the trailing edge and propagates from the wing to the center body. From BWB-450 to N2A, it can be seen that the center body of BWB is changed from "short and wide" to "long and narrow." This is because the shock wave is easy to generate at the "short and wide" center body, reducing the effective area of the wing and adversely affecting the high aerodynamic efficiency of the BWB [29]. Meanwhile, the "short and wide" center body will make it difficult to arrange the passenger cabin, cargo space, and the emergency evacuation of airplane personnel.

Therefore, the length of the rear of the SWB center body is extended to increase the length of the center body. Since the increasing of sweep angle is a good way to improve the aircraft transonic aerodynamic efficiency, the sweep angle of the SWB is increased. The basic shapes of the original SWB and the improved new SWB (SWB N) are shown in Figure 12.

It is difficult for SWB N to obtain good aerodynamic performance only when the basic shape is improved. Aerodynamic shape optimization is a good way to improve the aerodynamic performance of SWB N [30, 31]. Therefore, the SWB N is optimized using the discrete adjoint method at Ma = 0.85, $\alpha = 1.5^\circ$. The adjoint method provides a more efficient method of calculation gradients, which is independent of the step size and of the number of design variables [32].

The discrete adjoint equations need to be constructed based on the flow governing equation. The residual error of the control equation R can be expressed as a function of the flow-field conservation variable W, grid coordinate X, and design variable β. The following is the convergent governing equation:

$$R = R(W(\beta), X(\beta)) = 0. \quad (2)$$

In aerodynamic optimization design, the objective function is generally aerodynamic coefficient or its combination, so it is also a function of flow-field variable W, grid coordinate X, and design variable β. Therefore,

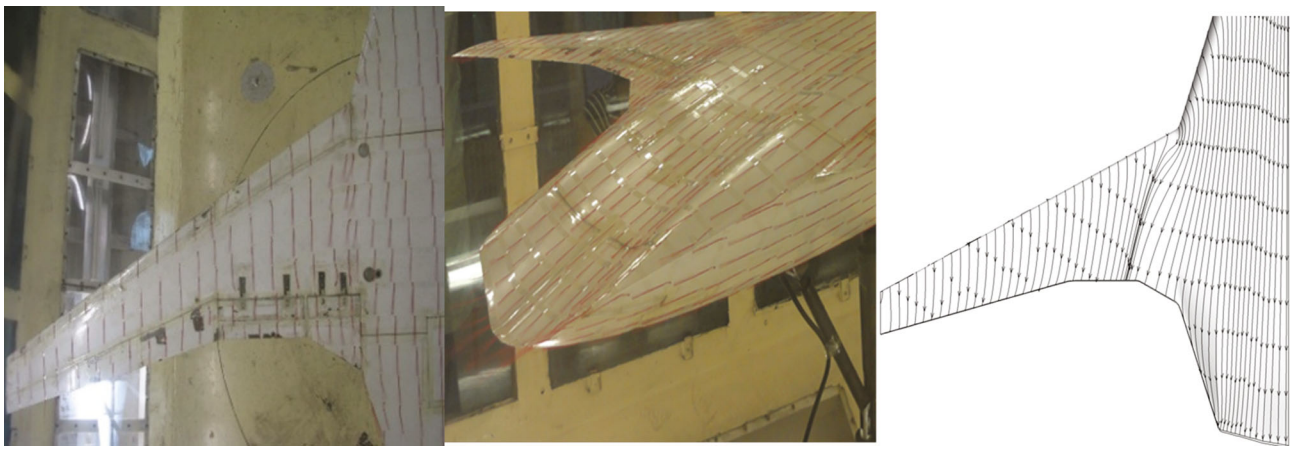

(a) $\alpha = 8^\circ$

(b) $\alpha = 10^\circ$

(c) $\alpha = 14^\circ$

Figure 8: Surface steam lines of SWB wind tunnel test and CFD results at take-off speed.

$$F = F(W(\beta), X(\beta)). \tag{3}$$

The following is the complete derivative of equations (2) and (3) on β:

$$\frac{dR}{d\beta} = \frac{\partial R}{\partial W}\frac{dW}{d\beta} + \frac{\partial R}{\partial X}\frac{dX}{d\beta} = 0, \tag{4}$$

$$\frac{dF}{d\beta} = \frac{\partial F}{\partial W}\frac{dW}{d\beta} + \frac{\partial F}{\partial X}\frac{dX}{d\beta}. \tag{5}$$

Bring equations (4) to (5):

$$\frac{dF}{d\beta} = \left[\frac{\partial F}{\partial X} - \frac{\partial F}{\partial W}\left(\frac{\partial R}{\partial W}\right)^{-1}\frac{\partial R}{\partial X}\right]\frac{dX}{d\beta}. \tag{6}$$

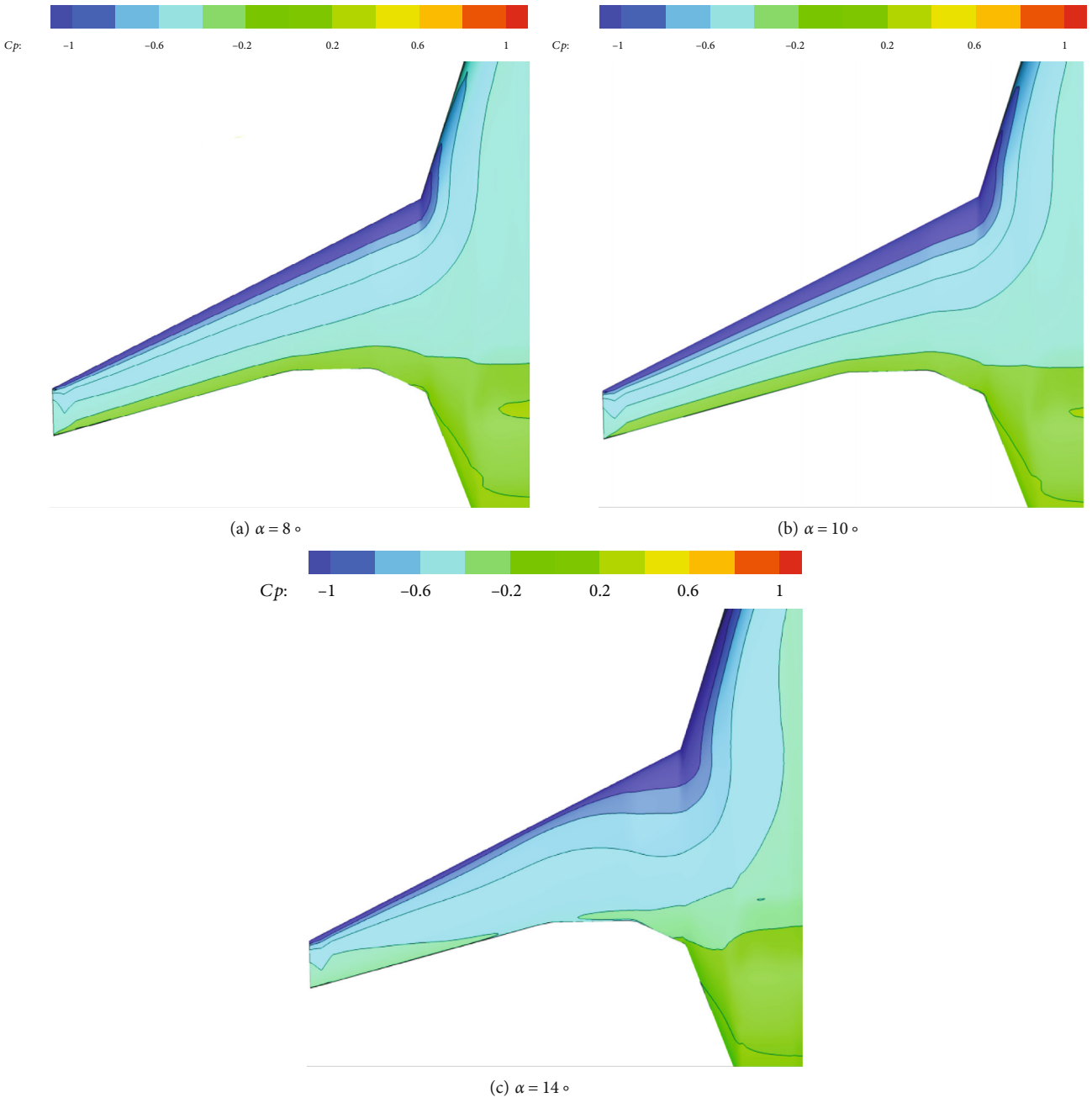

(a) $\alpha = 8^\circ$ (b) $\alpha = 10^\circ$

(c) $\alpha = 14^\circ$

Figure 9: Surface pressure contour of SWB at different angle of attack at take-off speed.

Solving equation (6) will involve solving the matrix inverse, and the cost of solving large-scale matrix inverse will be huge, so let the adjoint variable ψ be

$$\psi^T = \frac{\partial F}{\partial W}\left(\frac{\partial R}{\partial W}\right)^{-1}. \tag{7}$$

At this time, the matrix inversion calculation can be converted to the calculation of solving linear equations, that is, to solving the adjoint variable ψ from

$$\left(\frac{\partial R}{\partial W}\right)^T \psi = \left(\frac{\partial F}{\partial W}\right)^T. \tag{8}$$

Equation (6) can be written as

$$\frac{dF}{d\beta} = \left[\frac{\partial F}{\partial X} - \psi^T \frac{\partial R}{\partial X}\right]\frac{dX}{d\beta}. \tag{9}$$

This is how to use the discrete adjoint method to solve the gradient of aerodynamic objective function to design variables. General minimum residual (GMRES) [33, 34]

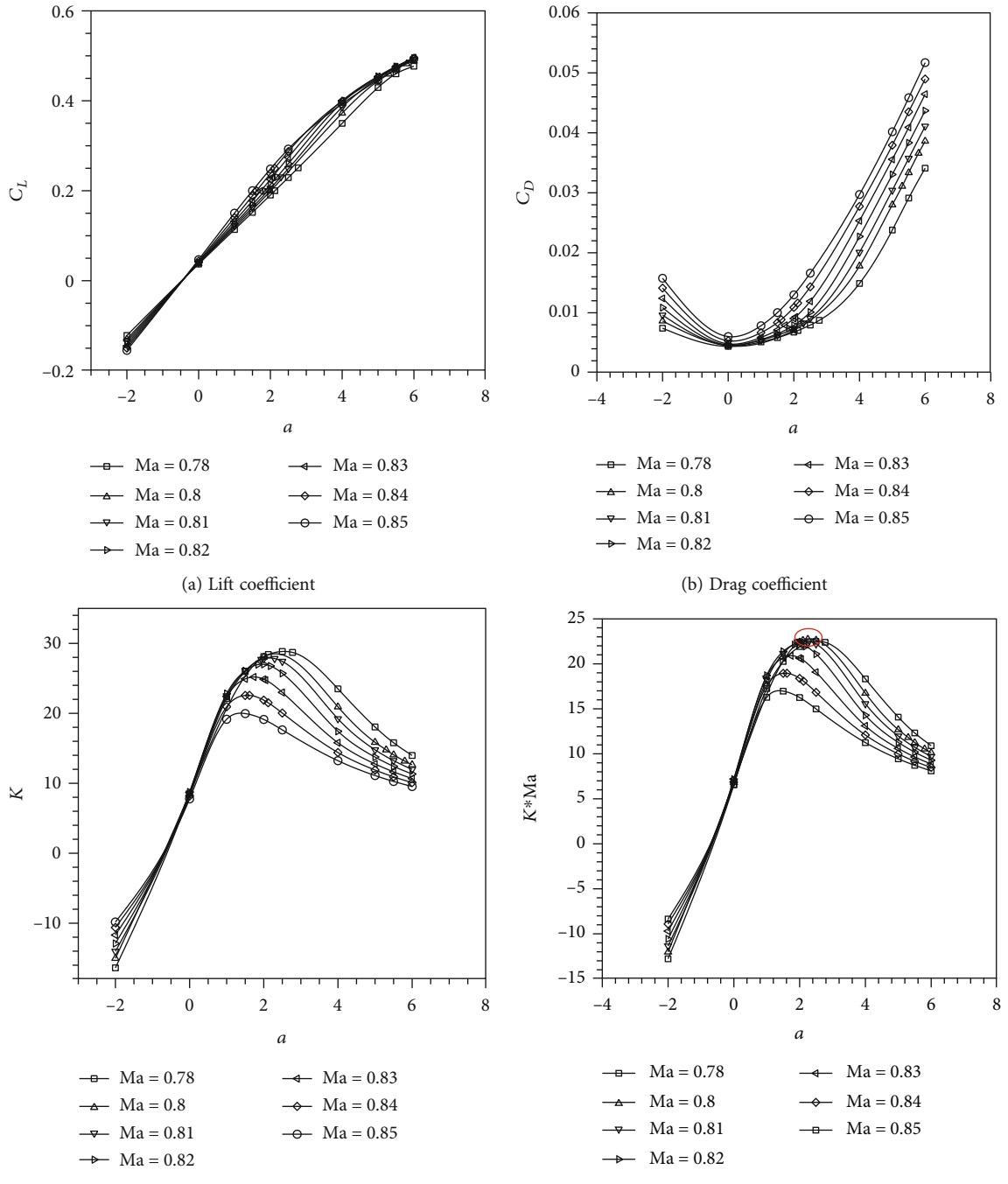

(a) Lift coefficient

(b) Drag coefficient

(c) Lift-to-drag ratio

(d) Aerodynamic efficiency factor

Figure 10: Continued.

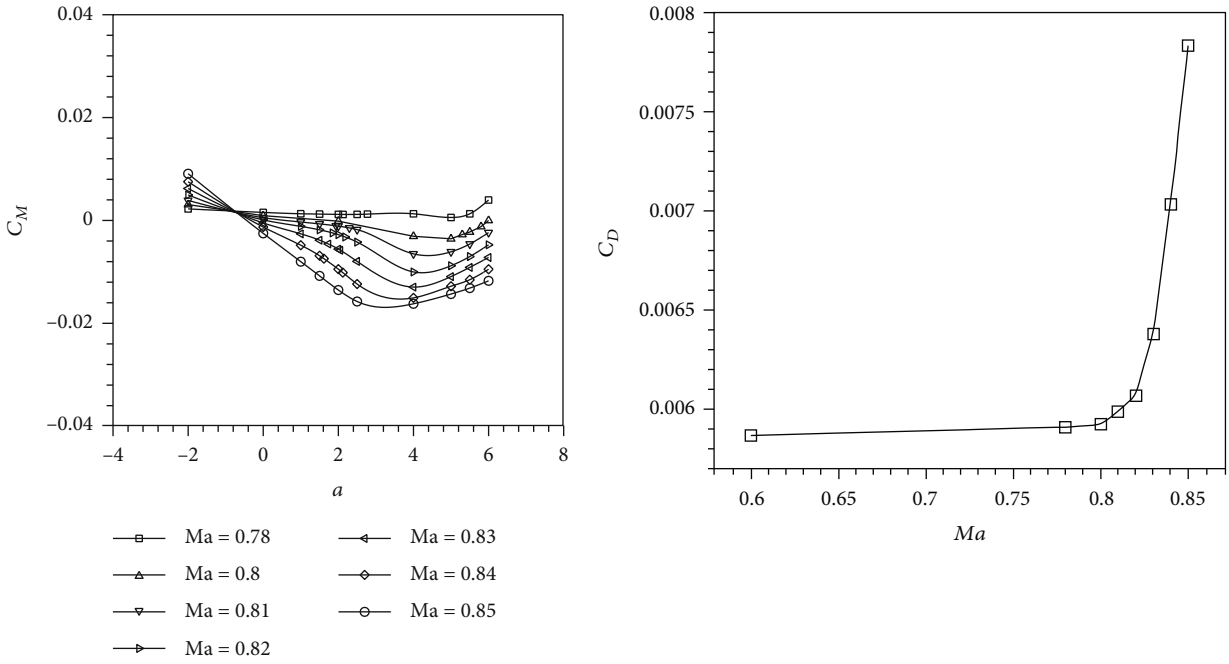

(e) Pitching moment coefficient

(f) Drag divergence

Figure 10: Typical aerodynamic characteristic curves of SWB at high speed.

method is applied to solve the adjoint equation. Sequential quadratic programming (SQP) [35] method is applied for optimization calculation. The freeform deformation (FFD) [36] method is applied as the surface parameterization and deformation method. In FFD, an initial box encapsulating the object to be redesigned is parameterized as a Bezier solid; a set of control points are defined on the surface of the box. The solid box is parameterized by the following expression:

$$X(u, v, w) = \sum_{i,j,k=0}^{l,m,n} P_{i,j,k} B_i^l(u) B_j^m(u) B_k^n(u), \qquad (10)$$

where $u, v, w \in [0, 1]$ and is the Bernstein polynomial of order. The Cartesian coordinates of the points on the surface of the object are then transformed into parametric coordinates with the Bezier box. The control points of the box become design variables, as they control the shape of the solid and thus the shape of the surface grid inside. The FFD box and control points used in SWB N optimization are shown in Figure 13. The airfoil shape, inclination angle, and twist angle can be adjusted by changing the position of control points.

The objective function is to reduce the drag at a given lift:

$$F = \omega_L \left(1 - \frac{C_L}{C_L^*}\right)^2 + \omega_D \left(1 - \frac{C_D}{C_D^*}\right)^2, \qquad (11)$$

where ω_L and ω_D are weight coefficients used to adjust the weights of lift and drag in the objective function, C_L^* is the target lift coefficient to be maintained, and C_D^* is one order smaller than the initial drag coefficient, similar to the initial resistance, but generally cannot be reached.

The final optimized shape is SWB ON. To distinguish it from SWB clearly, the SWB ON is named as SWB-2; the original SWB is named as SWB-1.

The surface pressure and streamlines of SWB-1 and SWB-2 at cruise speed (Ma = 0.85), $\alpha = 1.5^\circ$, are shown in Figure 14. It can be seen that due to the shape improvement, the shock wave on the upper surface is moved from the center body and trailing edge to the leading edge of the wing, thus improving the aerodynamic performance of SWB-2 at $\alpha = 1.5^\circ$.

The aerodynamic coefficient results of CFD analysis about SWB-1 and SWB-2 at cruise speed are shown in Figure 15. It can be seen that both configurations reach the maximum lift-to-drag ratio at $\alpha = 1.5^\circ$, and the $K_{\max}$ of SWB-2 at cruise Mach number is about 12% larger than that of SWB-1. Therefore, due to the improvement of the shape, the aerodynamic efficiency of the basic configuration is increased about 12% at $\alpha = 1.5^\circ$. However, the static margin of SWB is reduced, but it still meets the static stability requirements.

The aerodynamic coefficient results of CFD analysis about SWB-1 and SWB-2 at take-off speed (0.2 Ma) are shown in Figure 16. It can be seen from the results that the take-off speed aerodynamic performance of SWB-2 is also better than that of SWB-1. Moreover, compared with SWB-1, the static margin of SWB-2 is reduced at take-off speed. However, the maximum C_L of SWB-2 at take-off speed is only about 3 times of the C_L under cruise condition; it cannot satisfy the high- and low-speed coordinated design (about 5 times required).

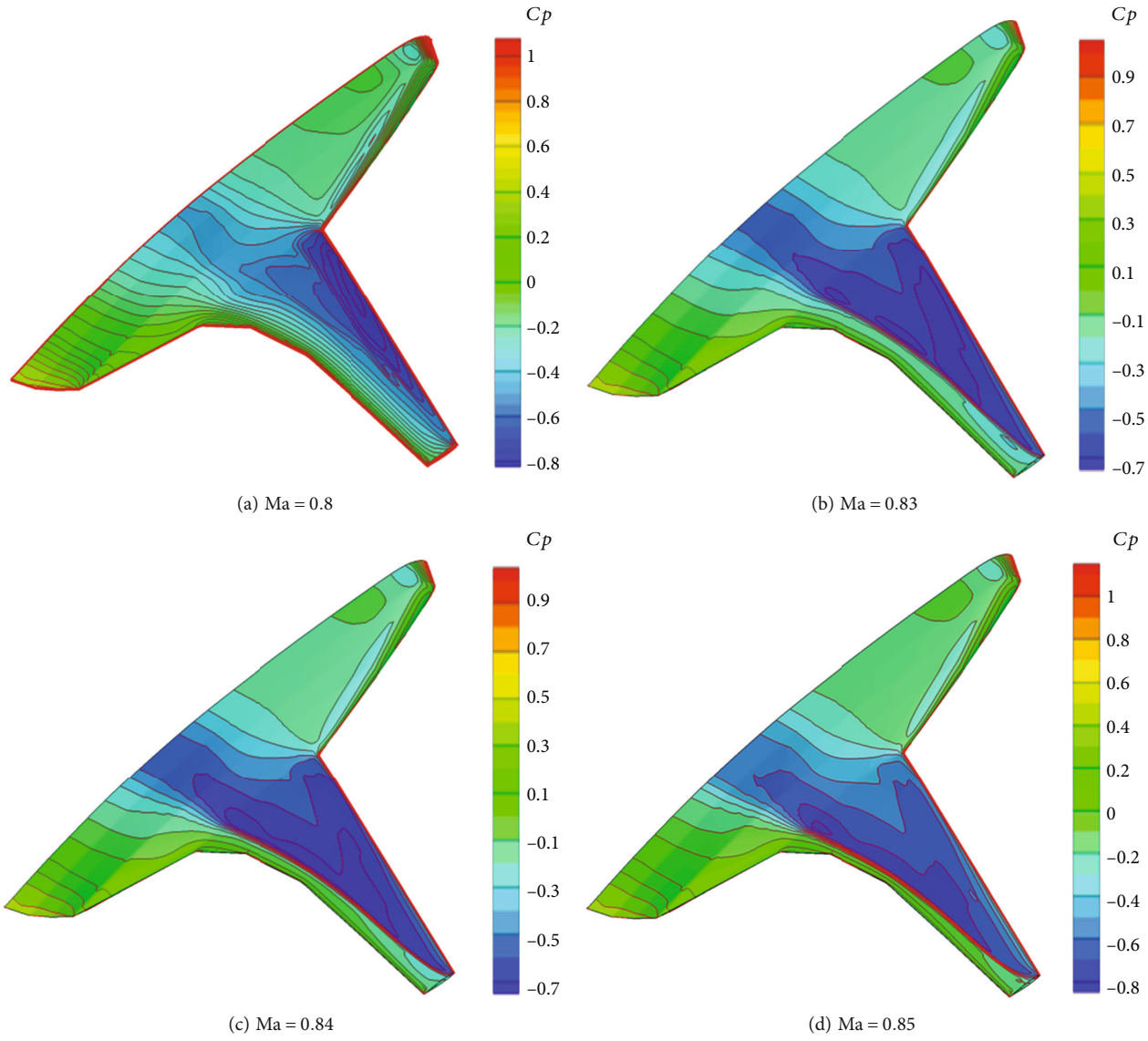

Figure 11: Surface pressure contour of SWB at different Mach number at $C_L = 0.2$.

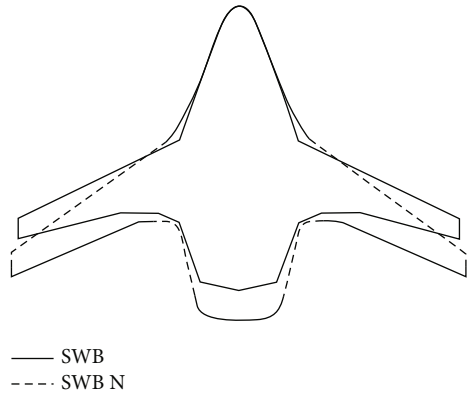

Figure 12: The basic shape of SWB and SWB N.

3.2. Winglets Added. Although the aerodynamic performance of SWB-1 is improved by 15% through the basic shape improvement, the result is still not very satisfactory. A way to continue to improve its aerodynamic performance needs to be found.

A winglet is a device used to improve the efficiency of an aircraft by lowering the lift-induced drag caused by wingtip vortices [37]. At present, winglets are commonly used in high-speed transport airplanes to increase its fuel efficiency. The winglets can increase the range of an airplane by as much as 7% at cruise speed. In general, any wingtips that do not end the wing simply horizontally are considered as some kind of a winglet, such as blended winglets, wingtip fence, and raked wingtip [38]. The blended winglets are used in SWB-2 to continue improve its aerodynamic performance.

The geometric parameters of the blended winglet include height (H), leading edge sweep angle (θ), taper ratio (Ct/Cr), and inclination angle (γ), as shown in Figure 17. The initial

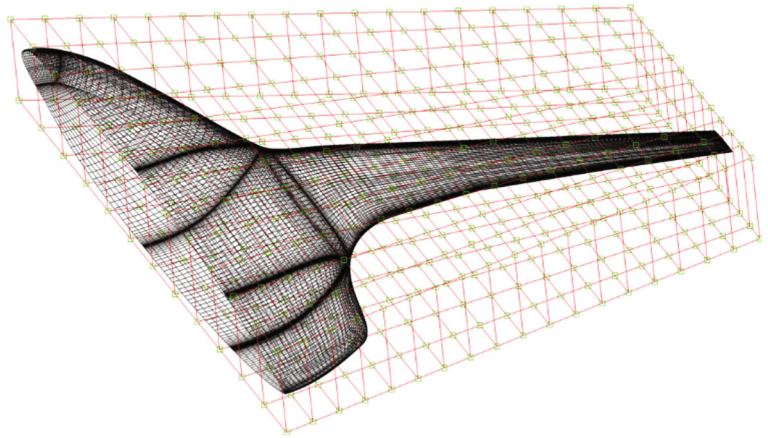

Figure 13: FFD box of SWB N.

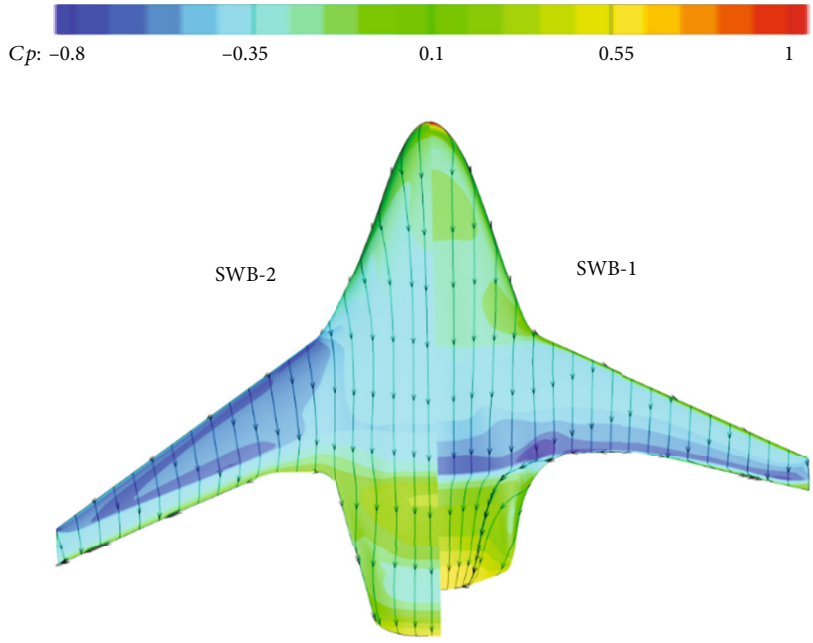

Figure 14: The surface pressure and streamlines of SWB-1 and SWB-2 at cruise speed, $\alpha = 1.5^\circ$.

shape of the winglet can be obtained by lofting the BWB wingtip airfoil according to these parameters. The blended winglets are attached to the wing with a smooth curve. Then, it is optimized using the discrete adjoint method based on FFD parameterization method as described in Section 3.1.

The shape of optimized winglet and SWB-2 with winglets is shown in Figure 18. To distinguish the basic configuration of SWB-2 from it with winglets, they are called SWB-2 BC (basic configuration) and SWB-2 WC (winglet configuration), respectively.

The lift-to-drag ratio and $C_L - C_D$ curve of CFD analysis about SWB-2 BC and SWB-2 WC at cruise speed are shown in Figure 19. It can be seen that the addition of winglets increases the lift-to-drag ratio of SWB-2 BC at the cruise angle of attack. And at the fixed value of C_L, the value of C_D of SWB-2 WC is always smaller than that of SWB-2 BC. It indicates that the winglets reduce the lift-induced drag well.

The surface pressure and streamlines of SWB-2 WC and BC at high speed, $\alpha = 1.5^\circ$, are shown in Figure 20. It can be seen that the surface pressure of the SWB-2 WC and BC is similar. Therefore, the influence of the added winglets is not obvious. However, the surface streamlines of the SWB-2 WC deviate towards the wing. It indicates that the winglets slightly increase the cross flow on the surface.

At take-off speed, the addition of winglets changes the aerodynamic performance of SWB-2 BC a little. Hence, this is not described in detail here.

3.3. High-Lift Device Added. The high-lift device is a key technology for civil aircraft to increase taking-off weight, shorten taking-off and landing distances, enhance airport

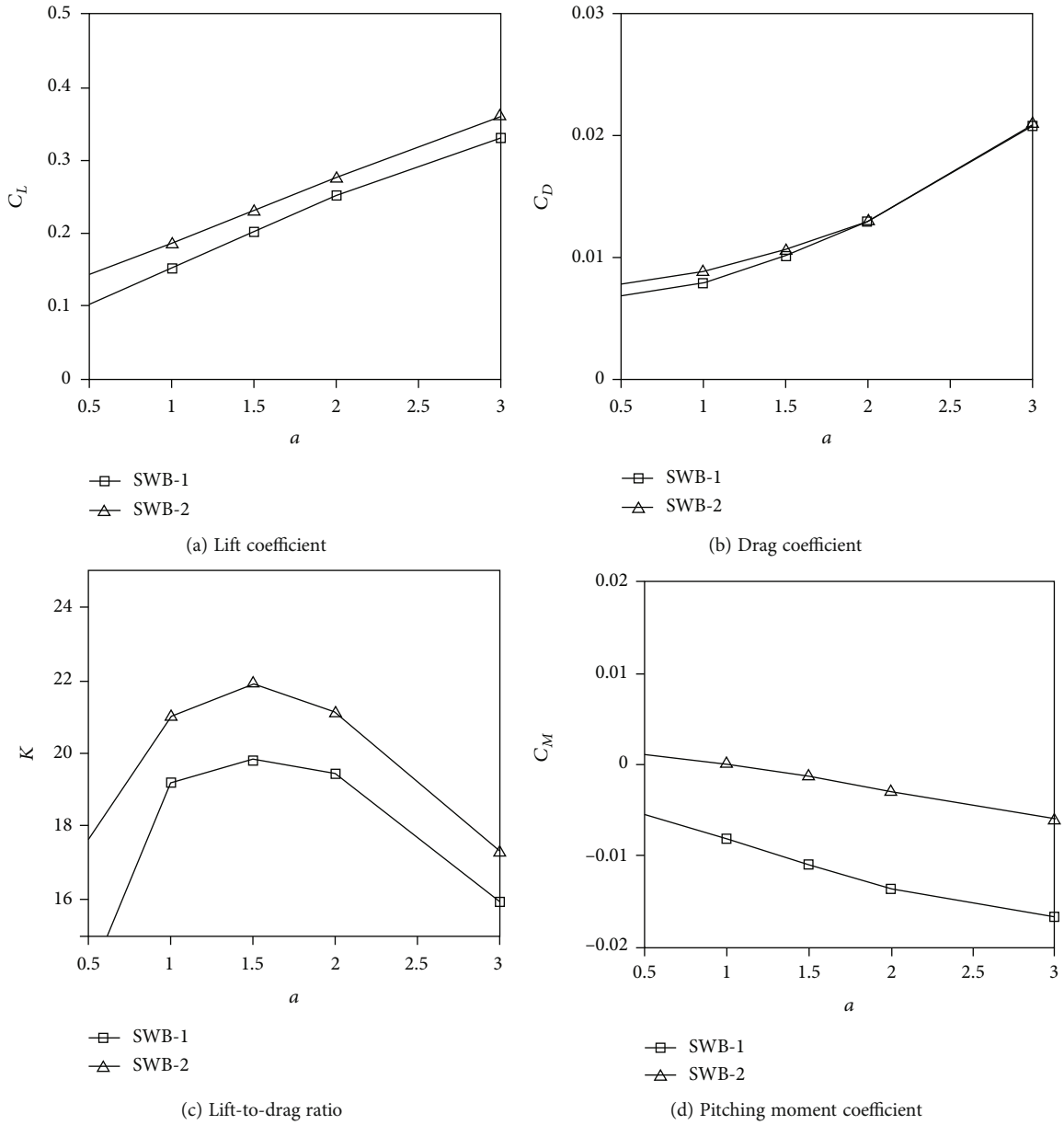

Figure 15: Cruise speed aerodynamic performance compared with SWB-1 and SWB-2.

adaptability, and coordinate high- and low-speed performance [39]. The traditional high-lift devices represented by the three-stage lifting device (composed of leading edge slat and trailing edge slotted flap) has obvious lifting effect, but the additional moment caused by it is large and is difficult to balance [40]. As the BWB is a high integration configuration, it has inherent shortcomings of short longitudinal control surface force and low trim efficiency [41]. Therefore, the traditional high-lift devices are difficult to be applied to BWB. Moreover, as an advantage configuration, hybrid/natural laminar flow (H/NLF) technology is expected to be applied in BWB, but the traditional high-lift devices will destroy the continuity of the upper surface of the wing [42].

Krueger flaps are proposed as early as 1947 by Krueger. However, they are not very practical until the laminar flow technology and the new configuration such as BWB appear. Kruger flaps are arranged on the lower surface of the front part of the wing, and the rotary motion mechanism along the leading edge is adopted to avoid damaging the continuity between the leading edge and the upper surface of the wing; in the take-off and landing phase, the deployed Kruger flaps not only have the effect of increasing lift but also have the effect of shielding the leading edge of the wing, which can prevent insects and dust contamination, and are suitable for the design of laminar flow wings. In ERA project, the BWB with Krueger flaps is designed and tested at take-off speed [43].

The design parameters of Krueger flaps include shape parameters and flap parameters as shown in Figure 21. The geometry of Krueger flaps head is a spline curve formed by

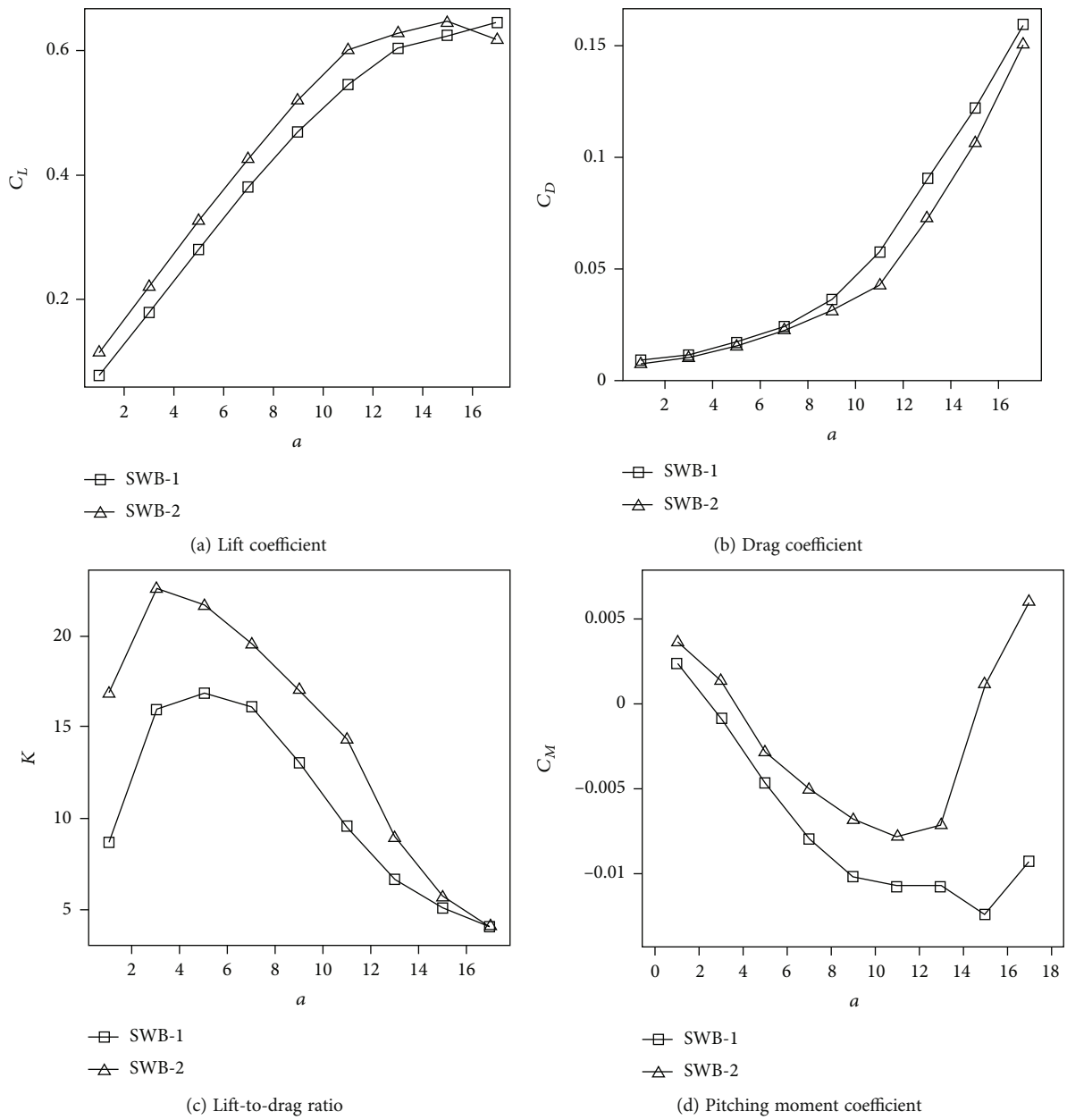

Figure 16: Take-off speed aerodynamic performance compared with SWB-1 and SWB-2.

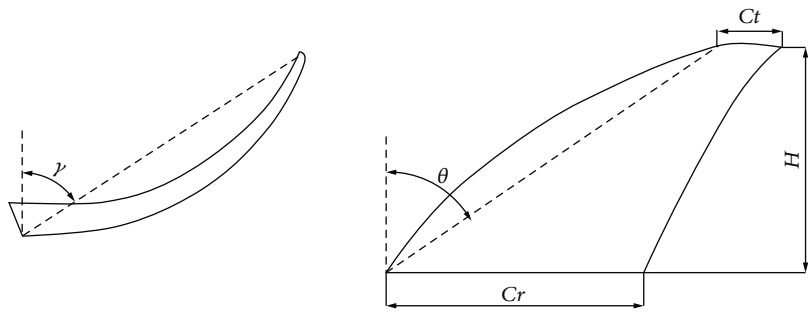

Figure 17: The geometric parameters of blended winglets.

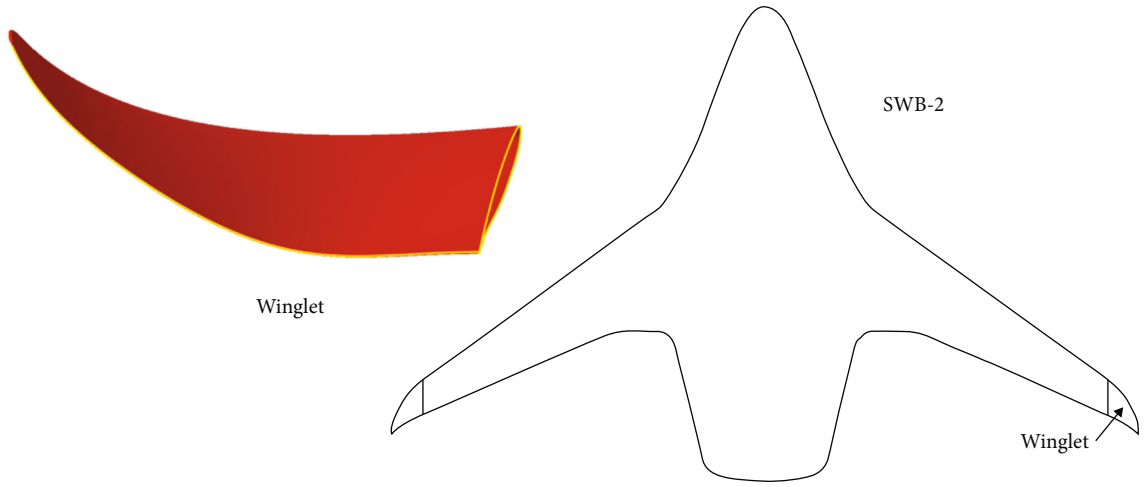

Figure 18: The shape of winglet and SWB-2 with winglets.

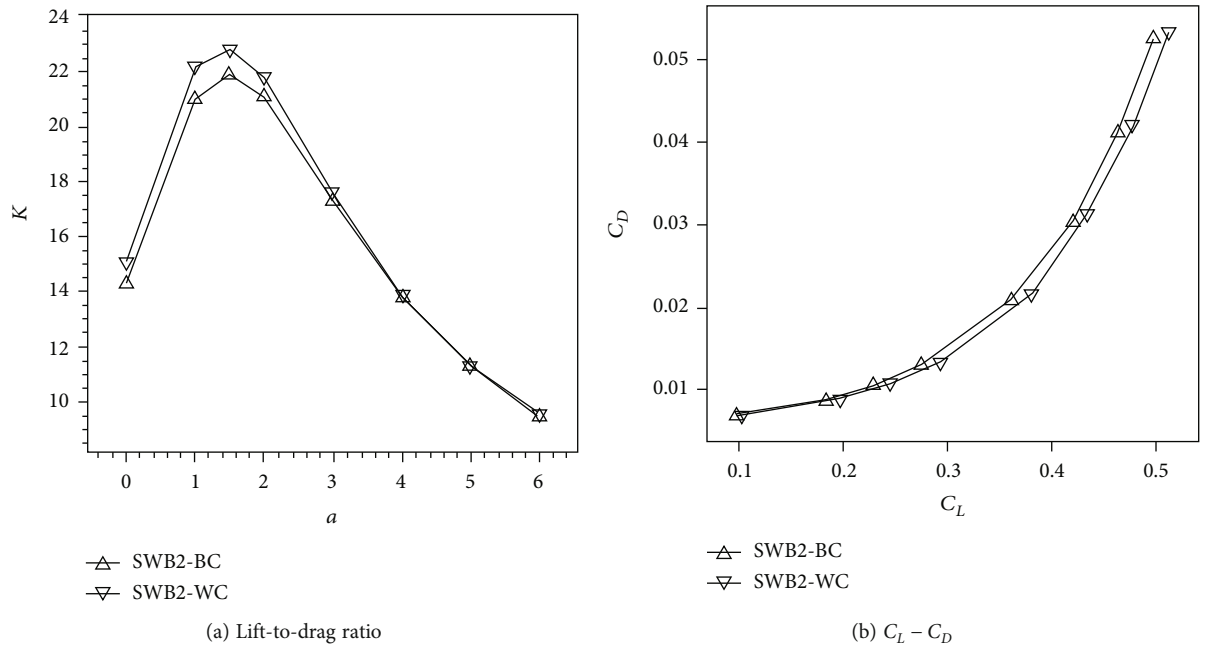

(a) Lift-to-drag ratio

(b) $C_L - C_D$

Figure 19: Cruise speed aerodynamic performance compared with SWB-2 BC and WC.

four control points k_1, k_2, k_3, and k_4; k_1 is the head start point, k_2 is the head leading edge point, k_3 is the head lower surface maximum thickness point, and k_4 is head end point. The curve between K_{start} and k_1 on the lower surface of the wing is the curve behind the head on the upper surface of the Krueger flaps. The flap parameters consist of hinge position (H_x, H_y) and deflection angle θ. Based on a response surface method (RSM) that relies on a regression kriging approach [44], the Krueger flaps are designed and applied to the SWB-2.

The Krueger flaps at the leading edge and simple flaps at the trailing edge constitute the high-lift device of SWB-2, as shown in Figure 22. The SWB-2 WC with high-lift device is called as SWB-2 HL.

The aerodynamic performance of SWB-2 WC and SWB-2 HL at landing and take-off states has been tested in the AVIC ARI FL-51 wind tunnel using a 1 : 22 scaled model (as shown in Figure 23) at $\text{Re} = 5.5 \times 10^6$. The wind tunnel results are shown in Figure 24. The results show that the three configurations have good stall and pitch moment performance. The high-lift device combined with leading edge Krueger flaps and trailing edge simple flaps can meet the take-off and landing lift requirements, and the low head moment increment is within the controllable range of the longitudinal control surface.

The surface pressure and streamlines of SWB-2 HL (take-off state) and WC at $\text{Ma} = 0.2$, $\alpha = 15^\circ$, are shown in Figure 25. It can be seen that, at $\alpha = 15^\circ$, the surface flow

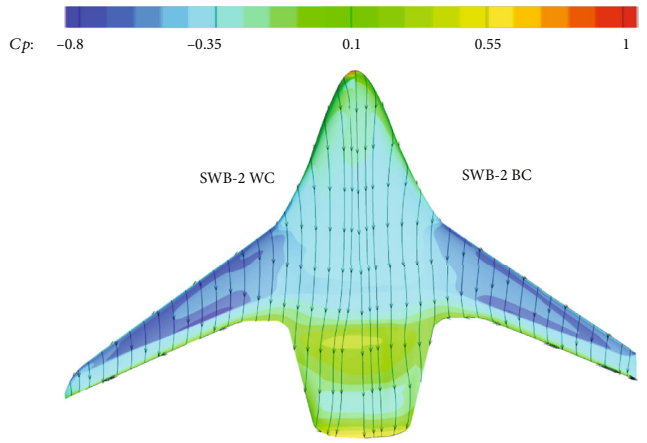

Figure 20: The surface pressure and streamlines of SWB-2 WC and BC at cruise speed, $\alpha = 1.5^{\circ}$.

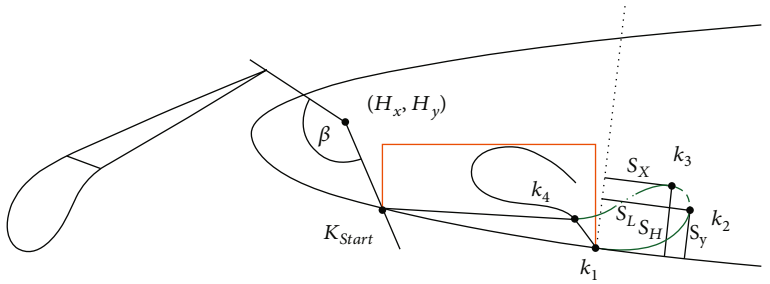

Figure 21: The design parameters of Krueger flaps.

Figure 22: The shape of SWB-2 with high-lift device.

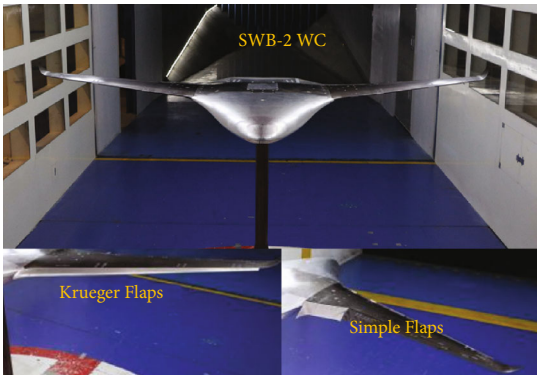

Figure 23: Wind test model of SWB-2 WC with Krueger flaps and simple flaps.

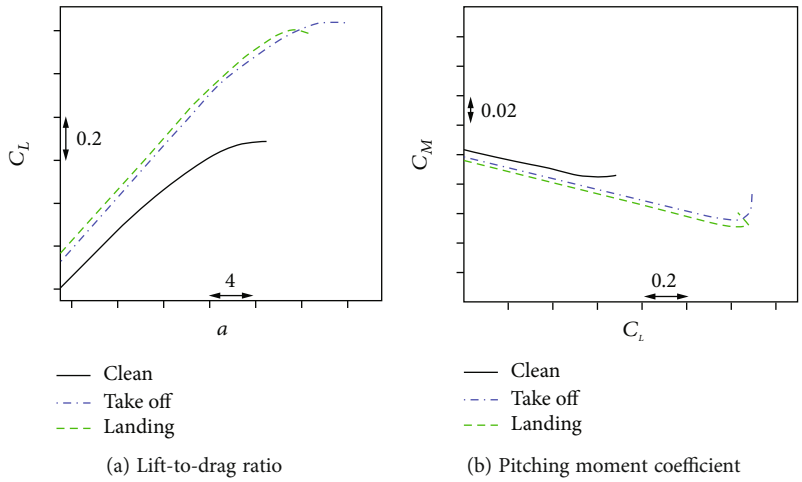

(a) Lift-to-drag ratio (b) Pitching moment coefficient

Figure 24: Aerodynamic performance compared with SWB-2 WC and HL at take-off speed.

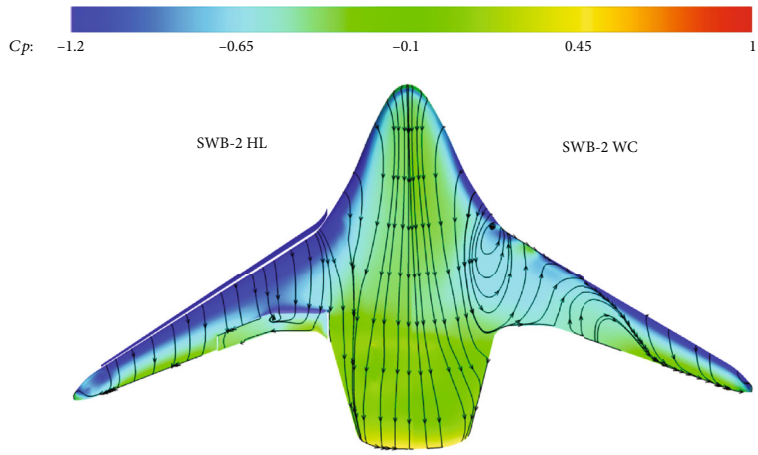

Figure 25: The surface pressure and streamlines of SWB-2 HL and BC at Ma = 0.2, $\alpha = 15^\circ$.

of SWB-2 WC is completely separated, but through the installation of Kruger flaps, the surface flow becomes the attached flow. Therefore, the Kruger flaps can improve the SWB-2 aerodynamic performance well.

4. Conclusions

In general, this paper solves the problem that the cruise aerodynamic performance of SWB becomes worse due to the increase of cruise Mach number by improving the planform shape and optimization design; the cruise aerodynamic performance of SWB is further improved by adding winglets; in addition, it also improves the low-speed take-off and landing performance of SWB by designing high-lift devices consisting of leading edge Krueger flaps and trailing edge simple flaps.

The CFD calculations and wind tunnel test results indicate that these improvement methods are appropriate and effective for improving the aerodynamic performance of BWB. Therefore, it shows a clear and meaningful way to increase the BWB cruise Mach number and to improve the BWB aerodynamic performance at cruise speed and take-off speed.

Data Availability

All data included in this study are available upon request by contact with the corresponding author.

Conflicts of Interest

The authors declare that they have no conflicts of interest.

References

[1] R. H. Liebeck, "Design of the blended wing body subsonic transport," *Journal of Aircraft*, vol. 41, no. 1, pp. 10–25, 2004.

[2] P. Dehpanah and A. Nejat, "The aerodynamic design evaluation of a blended-wing-body configuration," *Aerospace Science and Technology*, vol. 43, no. 3, pp. 96–110, 2015.

[3] C. Humphreys-Jennings, I. Lappas, and D. M. Sovar, "Conceptual design, flying, and handling qualities assessment of a

blended wing body (BWB) aircraft by using an engineering flight simulator," *Aerospace*, vol. 7, no. 5, p. 51, 2020.

[4] N. Qin, A. Vavalle, A. Le Moigne, M. Laban, K. Hackett, and P. Weinerfelt, "Aerodynamic considerations of blended wing body aircraft," *Progress in Aerospace Science*, vol. 40, no. 6, pp. 321–343, 2004.

[5] M. Weil Brenner, J. Trepanier, C. Tribes, and E. Petro, "Conceptual design framework for blended wing body airplane," in *12th AIAA Aviation Technology, Integration, and Operations (ATIO) Conference and 14th AIAA/ISSMO Multidisciplinary Analysis and Optimization Conference*, Indianapolis, Indiana, USA, 2012.

[6] L. T. Leifsson, *Multidisciplinary Design Optimization of Low-Noise Transport Aircraft, [Ph.D. Thesis]*, Virginia Polytechnic Institute and State University, 2006.

[7] P. Okonkwo and H. Smith, "Review of evolving trends in blended wing body aircraft design," *Progress in Aerospace Science*, vol. 82, pp. 1–23, 2016.

[8] R. Martinez-Val, C. Cuerno, E. Perez, and H. H. Ghigliazza, "Potential effects of blended wing bodies on the air transportation system," *Journal of Aircraft*, vol. 47, no. 5, pp. 1599–1604, 2010.

[9] S. Durmus, "A key design parameter proposal for aerodynamically efficient subsonic blended wing body," *Aircraft Engineering and Aerospace Technology*, vol. 94, no. 3, pp. 473–479, 2022.

[10] G. Wang, M. Zhang, Y. Tao et al., "Research on analytical scaling method and scale effects for subscale flight test of blended wing body civil aircraft," *Aerospace Science and Technology*, vol. 106, article 106114, 2020.

[11] Z. Xin, Z. Chen, W. Gu, M. Zhang, and B. Zhang, "Externally blown elevon applied for the longitudinal control of blended wing body transport with podded engines," *Aerospace Science and Technology*, vol. 93, article 105324, 2019.

[12] S. Siouris and N. Qin, "Study of the effects of wing sweep on the aerodynamic performance of a blended wing body aircraft," *Proceedings of the Institution of Mechanical Engineers, Part G: Journal of Aerospace Engineering*, vol. 221, no. 1, pp. 47–55, 2007.

[13] J. Gauvrit-Ledogar, S. Defoort, A. Tremolet, and F. Morel, "Multidisciplinary overall aircraft design process dedicated to blended wing body configurations," in *2018 Aviation technology, Integration, and Operations Conference*, Atlanta, Georgia, 2018.

[14] M. Carter, D. Vicroy, and D. Patel, "Blended-wing-body transonic aerodynamics: summary of ground tests and sample results (invited)," in *47th AIAA Aerospace Sciences Meeting including The New Horizons Forum and Aerospace Exposition*, Orlando, Florida, 2009.

[15] S. Wakayama, "Multidisciplinary design optimization of the blended-wing-body," in *7th AIAA/USAF/NASA/ISSMO Symposium on Multidisciplinary Analysis and Optimization*, p. 4938, St. Louis, MO, U.S.A, 1998.

[16] A. Diedrich, J. Hileman, D. Tan, K. Willcox, and Z. Spakovszky, "Multidisciplinary design and optimization of the silent aircraft," in *44th AIAA Aerospace Sciences Meeting and Exhibit*no. 1323, pp. 1–12, Reno, Nevada, 2006.

[17] L. Ng, *Design and Acoustic Shielding Prediction of Hybrid Wing-Body Aircraft, [M.S. Thesis]*, Dept. of Aeronautics and Astronautics Massachusetts Institute of Technology, Cambridge, MA, 2009.

[18] H. Kim and M. S. Liou, "Flow simulation of n2b hybrid wing body configuration,," in *50th AIAA Aerospace Sciences Meeting including the New Horizons Forum and Aerospace Exposition*, Nashville, Tennessee USA, 2012.

[19] M. Brown and R. Vos, "Conceptual design and evaluation of blended-wing body aircraft," in *2018 AIAA Aerospace Sciences Meeting*, Kissimmee, Florida, 2018.

[20] Z. Chen, M. Zhang, Y. Chen et al., "Assessment on critical technologies for conceptual design of blended-wing-body civil aircraft," *Chinese Journal of Aeronautics*, vol. 32, no. 8, pp. 1797–1827, 2019.

[21] G. Yu, D. Li, and Z. Zhang, "Numerical simulation for the differences between FTN/WPN engine models aerodynamic influence on BWB300 airframe," *Engineering Applications of Computational Fluid Mechanics*, vol. 14, no. 1, pp. 566–579, 2020.

[22] A. M. Ez Abadi, M. Sadi, M. Farzaneh-Gord, M. H. Ahmadi, R. Kumar, and K. Chau, "A numerical and experimental study on the energy efficiency of a regenerative heat and mass exchanger utilizing the counter-flow Maisotsenko cycle," *Engineering Applications of Computational Fluid Mechanics*, vol. 14, no. 1, pp. 1–12, 2020.

[23] J. I. Hileman, Z. S. Spakovszky, M. Drela, M. A. Sargeant, and A. Jones, "Airframe design for silent fuel-efficient aircraft," *Journal of Aircraft*, vol. 47, no. 3, pp. 956–969, 2010.

[24] P. Li, B. Zhang, Y. Chen, C. Yuan, and Y. Lin, "Aerodynamic design methodology for blended wing body transport," *Chinese Journal of Aeronautics*, vol. 25, no. 4, pp. 508–516, 2012.

[25] Y. Gang, L. Dong, C. Zhenli, and Z. Zeyu, "Blended wing body thrust reverser cascade feasibility evaluation through CFD," *IEEE Access*, vol. 7, pp. 155184–155193, 2019.

[26] R. Liebeck, "Blended wing body design challenges," in *AIAA International Air and Space Symposium and Exposition: The Next 100 Years*, Dayton, Ohio, 2003.

[27] S. Karpuk, Y. Liu, and A. Elham, "Multi-fidelity design optimization of a long-range blended wing body aircraft with new airframe technologies," *Aerospace*, vol. 7, no. 7, p. 87, 2020.

[28] M. Zhang, Z. Chen, Z. Tan et al., "Effects of stability margin and thrust specific fuel consumption constrains on multidisciplinary optimization for blended-wing-body design," *Chinese Journal of Aeronautics*, vol. 32, no. 8, pp. 1847–1859, 2019.

[29] D. Roman, R. Gilmore, and S. Wakayama, "Aerodynamics of high-subsonic blended-wing-body configurations," in *41st Aerospace Sciences Meeting and Exhibit*, Reno, Nevada, 2003.

[30] Z. Lyu and J. R. R. A. Martins, "Aerodynamic shape optimization of a blended-wing-body aircraft," in *51st AIAA Aerospace Sciences Meeting including the New Horizons Forum and Aerospace Exposition*, Grapevine, Texas, January 2013.

[31] C. M. Boozer, M. J. Van Tooren, and A. Elham, "Multidisciplinary aerodynamic shape optimization of a composite blended wing body aircraft," in *58th AIAA/ASCE/AHS/ASC Structures, Structural Dynamics, and Materials Conference*, Grapevine, Texas, January 2017.

[32] R. Rashad and D. W. Zingg, "Aerodynamic shape optimization for natural laminar flow using a discrete-adjoint approach," *AIAA Journal*, vol. 54, no. 11, pp. 3321–3337, 2016.

[33] A. Le Moigne, *A Discrete Navier-Stokes Adjoint Method for Aerodynamic Optimisation of BlendedWing-Body Configurations, [Ph.D. thesis]*, Cranfield University, 2002.

[34] Y. Saad and M. H. Schultz, "GMRES: a generalized minimal residual algorithm for solving nonsymmetric linear systems," *SIAM Journal on Scientific and Statistical Computing*, vol. 7, no. 3, pp. 856–869, 1986.

[35] M. Fesanghary, M. Mahdavi, M. Minary-Jolandan, and Y. Alizadeh, "Hybridizing harmony search algorithm with sequential quadratic programming for engineering optimization problems," *Computer Methods in Applied Mechanics and Engineering*, vol. 197, no. 33-40, pp. 3080–3091, 2008.

[36] T. W. Sederberg and S. R. Parry, "Free-form deformation of solid geometric models," in *ACM SIGGRAPH Computer Graphics*, p. 20, New York, NY, United States, 1986.

[37] A. Elham and M. J. L. van Tooren, "Winglet design using multidisciplinary design optimization techniques," *AIP Conference Proceedings*, vol. 1618, p. 372, 2014.

[38] E. E. Khalil, H. Helal, O. Abdellatif, and G. M. ElHarriri, "Aircraft-blended winglet performance analyses," in *55th AIAA Aerospace Sciences Meeting*, Grapevine, Texas, January 2017.

[39] J. Mao and Y. Chen, "Study on optimization for high lift devices of civil aircraft based on rapid calculation method," *Journal of Physics: Conference Series*, vol. 1875, no. 1, article 012009, 2021.

[40] J. Bowlus, D. Multhopp, S. Banda, J. Bowlus, D. Multhopp, and S. Banda, "Challenges and opportunities in tailless aircraft stability and control," in *Guidance, Navigation, and Control Conference*, New Orleans, LA, U.S.A., 1997.

[41] Z. Chen, Q. Li, X. Ju, and F. Cen, "Barrier Lyapunov function-based sliding mode control for BWB aircraft with mismatched disturbances and output constraints," *IEEE Access*, vol. 7, pp. 175341–175352, 2019.

[42] P. Loechert, K. C. Huber, C. Liersch, and A. Schuette, "Control device studies for yaw control without vertical tail plane on a 53° swept flying wing configuration," in *2018 Applied Aerodynamics Conference*, Atlanta, Georgia, June 2018.

[43] D. D. Vicroy, E. D. Dickey, N. Princen, and M. Beyar, "Overview of low-speed aerodynamic tests on a 5.75% scale blended-wing-body twin jet configuration (invited)," in *54th AIAA Aerospace Sciences Meeting*, San Diego, California, USA, January 2016.

[44] G. Michele and J. Brezillon, "High lift devices design of a supersonic transport aircraft based on 3D computational fluid dynamics," in *6th European Congress on Computational Methods in Applied Sciences and Engineering*, Vienna, Austria, September 2012.